Analytical Propagation Solution for Planet-Displaced Orbit in the Presence of Third-body Perturbations

Xingyu Zhou[a,b], Dong Qiao[a,1], Xiangyu Li[a], Malcolm Macdonald[c]

[a] *School of Aerospace Engineering, Beijing Institute of Technology, Beijing, 100081, China*
[b] *Beijing Institute of Technology Chongqing Innovation Center, Chongqing, 401120, China*
[c] *Department of Electronic and Electrical Engineering, University of Strathclyde, Glasgow, G1 1XJ, UK*

Abstract

Planet-displaced orbits (PDOs) play an important role in space missions such as solar observation, gravitational wave detection, and near-Earth asteroid detection. To propagate the PDOs accurately and efficiently, this paper develops an analytical solution considering the Solar central gravitational force and the time-varying third-body perturbation of the corresponding planet. First, an approximated third-body perturbation model is established based on the planet displacement angle (PDA), which is found to be the core variable affecting the evolution of the orbit. The model can describe both secular and periodic terms of the third-body perturbation accurately. Then, based on the established third-body perturbation model, a two-step procedure is developed to iteratively derive the analytical orbit propagation solution of the PDO via the Picard iteration method. The analytical solution is successfully applied to propagate the orbit in an Earth-trailing orbit case: the Laser Interferometer Space Antenna (LISA). Simulation shows that the analytical orbit propagation solution can accurately predict the orbit in both the long-time and short-time cases. The relative error is less than 0.1% in 10 years. The proposed analytical solution can be potentially useful in designing and optimizing PDOs.

Email addresses: zhouxingyu@bit.edu.cn (Xingyu Zhou), qiaodong@bit.edu.cn (Dong Qiao), lixiangy@bit.edu.cn (Xiangyu Li), malcolm.macdonald.102@strath.ac.uk (Malcolm Macdonald)
[1] Corresponding Author

Keywords: Planet-displaced orbits, Picard iteration method, Third-body perturbation, Planet displacement angle, Analytical orbit propagation, LISA

1. Introduction

Planet-displaced orbits (PDOs) lead (planet-leading orbits, PLOs) or trail (planet-trailing orbits, PTOs) a planet in its orbit around the Sun. The PDOs are typically circular and coplanar with the planet. They have gained increasing attention for their considerable value in deep space exploration missions that require stable and reliable environments. For example, to name a few, the Earth-leading orbits for the solar observation [1], the Earth-trailing orbits (ETOs) for the gravitational wave detection [2, 3, 4, 5], and the Venus-displaced orbits for the near-Earth asteroid detection [6]. Accurate and efficient propagation of these PDOs is crucial in designing and optimizing them [3].

The motion of a PDO is essentially a three-body problem, as the gravitational forces acting on a spacecraft in a PDO are primarily caused by the Sun (*i.e.*, the primary body) and the planet (*i.e.*, the secondary body) it is leading or trailing [7]. Extensive researches have been conducted on the TBP [8, 9, 10], in which the circular restricted three-body problem (CRTBP) [11, 12, 13] and the elliptical restricted three-body problem (ERTBP) [14] are two fundamental models [15]. Pezent *et al.* utilized the CRTBP equation and a high-fidelity dynamical model to devise controlled periodic orbits around Earth-trailing equilibrium points [7]. They also examined the stability of a solar sail near-vertical ETO within the CRTBP framework and concluded that the solar sail near-vertical ETO is more stable than traditional sub-L1 sail-based vertical orbits [1]. The CRTBP and ERTBP models offer the advantage of determining equilibrium solutions for the TBP. However, the PDOs can only be numerically propagated under the CRTBP and ERTBP models, as neither the CRTBP nor the ERTBP has analytical solutions [16, 17]. Although numerical methods can accurately propagate the orbit, they suffer from drawbacks related to heavy computational overhead [18].

Analytical orbit propagation, on the other hand, can surpass numerical methods by providing explicit expressions for orbit states [19, 20]. These expressions can be extremely beneficial for onboard orbit control and uncertainty propagation [21, 22, 23, 24]. The challenge of deriving an analytical propagation solution for the PDOs lies in accounting for the time-varying perturbations acting on the spacecraft. A variety of analytical propagation methods have been developed for orbits under additional accelerations, such as perturbations and thrusts, which can be broadly classified into three groups.

The first group includes different orbital averaging techniques, which simplify the time-varying perturbations by averaging them. Cook proposed a first-order orbit propagation method for an Earth-orbiting spacecraft under luni-solar perturbations, assuming that the perturbations remain constant in one orbital revolution. The result is a semi-analytical solution of the orbital element variations in one revolution, and thus, repeated computations are required for long-term propagation as the positions of disturbing bodies (*i.e.*, the Sun and the Moon) differ in different orbital revolutions. Cook's theory applies primarily to cases when the distance between the spacecraft and the central body is much smaller than the distance between the disturbing and central bodies [25]. Paul further proposed a second-order solution for orbit propagation under third-body perturbations to improve the accuracy of Cook's first-order theory [26]. While their methods work well with Earth-orbiting scenarios, they are not suitable for PDOs due to the distance assumptions. In addition, their methods cannot capture short-term changes when propagating orbits as the third-body perturbations are averaged in each revolution.

The second group includes analytical orbit propagation solutions for some special cases, *e.g.*, the cases when the direction of the additional acceleration is fixed (*i.e.*, radial, circumferential, and tangential) [27] or when the magnitude of the additional acceleration remains constant [28, 29]. Tsien first developed an explicit solution for the case when the additional accelerations are constant and along the radial direction [30]; then, Tsien developed an approximated solution for the case when the thrusts are constant and circumferential [30].

Alternative analytical solutions for constant and radial cases are also derived in [31, 32]. In addition, approximated solutions are proposed by Benney [33] and Perkins [34] when the thrust accelerations are constant and tangential. More recently, Gurfil investigated the problem of spacecraft rendezvous using constant-magnitude thrust and developed a new solution [35]. Unfortunately, the third-body perturbations on the PDO spacecraft are neither direction-fixed nor magnitude-constant.

The third group contains several approximation-based methods to address general acceleration profiles [36], such as the Lie series [37, 38] and the Fourier series [39, 40]. Zhao and Lei utilized the Lie-series transformation method to construct an approximated analytical solution of invariant manifolds in the CRTBP [38]. Ko and Scheeres employed 14 thrust Fourier coefficients to approximate each component of the thrust accelerations [39]. Nie and Gurfil expressed Gauss's variational equations using the Fourier series in terms of the mean anomaly [41]. They neglect short-term orbital changes and can only capture secular variations. However, for applications such as gravitational wave detection, accurate propagation is required, and the periodic changes in the orbit cannot be ignored [42]. Thus, the motivation of this work is to provide an accurate analytical orbit propagation suitable for PDOs without neglecting periodic terms.

This paper proposes an analytical propagation solution for the PDOs under time-varying third-body perturbations. In contrast to the aforementioned orbital averaging techniques and approximation-based methods that only consider secular terms, one of the innovations is to consider both secular and periodic terms of PDOs. For this purpose, a third-body perturbation model for PDOs is first developed, in which the periodic effects of third-body perturbations on orbital motion are represented using the planet displacement angle. The other innovation of this work is, based on the idea of the Picard iteration method, proposing a two-step procedure to iteratively derive the analytical propagation solution under the developed third-body perturbation model. Both the orbit plane and eccentricity of the disturbing body are considered during the deriva-

tion process. With the above advantages at play, the proposed analytical orbit propagation is accurate for both long-term and short-term propagations.

The rest of this paper is organized as follows. Section 2 states the dynamics and the orbit propagation problem of the PDO. The third-body perturbation model is proposed in section 3. Section 4 derives the analytical solution. Numerical validation results are presented in section 5, and a potential application of the proposed analytical propagation solution is shown in 6. Finally, the conclusions are given in section 7.

2. Problem Statement

Consider a system with one central body, one disturbing body, and one spacecraft. The disturbing body is assumed to move around the central body in a Keplerian orbit with a small eccentricity. The spacecraft leads or trails the disturbing body in its orbit around the central body in a PDO. To investigate the motion of a spacecraft in the PDO, an inertial coordinate system, in which the origin is locates on the barycenter of the central body, the x-axis points to the vernal equinox, the z-axis is vertical to the orbit plane of the disturbing body, and the y-axis is defined by a right-handed coordinate system, is used. Obviously, the inclination of the disturbing body is zero in the defined inertial coordinate system. The PDO spacecraft is assumed to move on a near-circular orbit with a small inclination. Moreover, the semi-major axis of the spacecraft is assumed to be close to that of the disturbing body. An example in the Sun-Earth system, *i.e.*, the Earth-trailing orbit (ETO), is shown in Figure 1.

The orbit state of the spacecraft is represented by the Keplerian orbit elements, given by

$$\boldsymbol{K} = [a, e, i, \Omega, \omega, \theta]^T \tag{1}$$

where a, e, i, Ω, ω and θ are the semi-major axis, eccentricity, inclination, right ascension of the ascending node (RAAN), argument of periapsis, and true anomaly of the spacecraft, respectively. According to Lagrange's planetary equations [15], the motion of the spacecraft is described using a series of

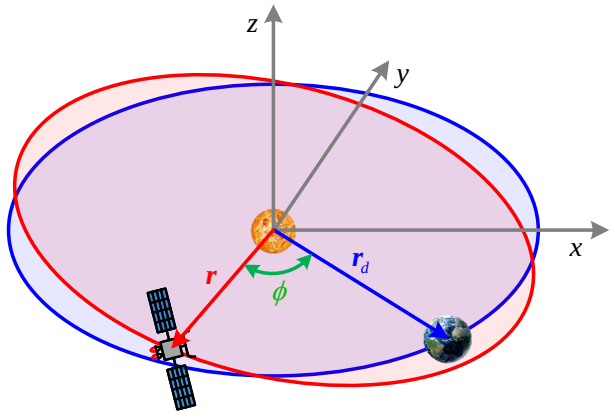

Figure 1: An illustration of the Earth-trailing orbit.

ordinary differential equations (ODEs) as

$$\begin{cases} \dfrac{da}{dt} = \dfrac{2}{n\sqrt{1-e^2}}\left[Re\sin\theta + \dfrac{a}{r}\left(1-e^2\right)S\right] \\ \dfrac{de}{dt} = \dfrac{\sqrt{1-e^2}}{na}[R\sin\theta + S(\cos\theta + \cos E)] \\ \dfrac{di}{dt} = \dfrac{Wr\cos u}{na^2\sqrt{1-e^2}} \\ \dfrac{d\Omega}{dt} = \dfrac{Wr\sin u}{na^2\sqrt{1-e^2}\sin i} \\ \dfrac{d\omega}{dt} = \dfrac{\sqrt{1-e^2}}{nae}\left[-R\cos\theta + \left(1 + \dfrac{r}{a\left(1-e^2\right)}\right)S\sin\theta - \dfrac{er}{a\left(1-e^2\right)}W\cot i\sin u\right] \\ \dfrac{du}{dt} = \dfrac{na^2\sqrt{1-e^2}}{\gamma r^2} \end{cases} \tag{2}$$

where $\frac{1}{\gamma} = 1 - \frac{Wr^3\cot i\sin u}{n^2a^4(1-e^2)} = 1 - \frac{d\Omega}{du}\cos i$, $u = \theta + \omega$ is the argument of the latitude; n denotes the mean angular motion of the spacecraft; E is the eccentric anomaly; r is the radial distance; and R, S, and W represent the components of the disturbing acceleration along the radial, circumferential, and normal directions, respectively. In this paper, the suffix 0 denotes the state of the spacecraft at the initial epoch, and the suffix d denotes the state of the

disturbing body. Then, the problem is described as follows: given the initial orbit elements $\boldsymbol{K}_0 = [a_0, e_0, i_0, \Omega_0, \omega_0, \theta_0]^T$ at the initial epoch t_0, find a solution of orbit elements $\boldsymbol{K}$ satisfying the ODEs in Eq. (2).

According to [15], the changes in Ω and ω can be neglected considering only third-body perturbations. Thus, we have $\gamma \approx 1$ and $\frac{du}{d\theta} = 1 + \frac{d\omega}{d\theta} \approx 1$. Then, the ODEs in Eq. (2) can be replaced with ODEs with respect to θ, yielding

$$\begin{cases} \dfrac{da}{d\theta} = \dfrac{2r^2}{n^2a^2\left(1-e^2\right)}\left[Re\sin\theta + \dfrac{a}{r}\left(1-e^2\right)S\right] \\ \dfrac{de}{d\theta} = \dfrac{r^2\sqrt{1-e^2}}{n^2a^3}[R\sin\theta + S(\cos\theta + \cos E)] \\ \dfrac{di}{d\theta} = \dfrac{Wr^3\cos u}{n^2a^4\left(1-e^2\right)} \\ \dfrac{d\Omega}{d\theta} = \dfrac{Wr^3\sin u}{n^2a^4\left(1-e^2\right)\sin i} \\ \dfrac{d\omega}{d\theta} = \dfrac{r^2}{n^2a^3e}\left[-R\cos\theta + \left(1 + \dfrac{r}{a\left(1-e^2\right)}\right)S\sin\theta - \dfrac{er}{a\left(1-e^2\right)}W\cot i\sin u\right] \end{cases} \tag{3}$$

Additionally, in the defined inertial coordinate system, several assumptions are made for the PDOs. First, the inclination of the disturbing body is 0 (*i.e.*, $i_d = 0$), and the eccentricity of the disturbing body is small (*i.e.*, $e_d \approx 0$). Second, the inclination and the eccentricity of the spacecraft are small (*i.e.*, $i \approx 0$ and $e \approx 0$). In the succeeding derivation process, the terms of i (including $\sin i$) and e can be ignored if a much larger quantity exists. For example, the term $1 - e^2$ can be approximated by 1. It should be noted that, as the classic Keplerian orbit elements are employed (see Eqs. (1)-(3)), the eccentricity of the spacecraft cannot be zero; otherwise, ω is not well defined. Third, the semi-major axis of the spacecraft is approximately equal to that of the disturbing body (*i.e.*, $a \approx a_d$). Combined with the assumptions of $e_d \approx 0$ and $e \approx 0$, we have $r \approx r_d$. Based on the assumptions above, the analytical solution for the PDO is derived in the following two sections.

3. Third-Body Gravitational Perturbation Model

Let $\boldsymbol{r} = [x, y, z]^T$ and $\boldsymbol{r}_d = [x_d, y_d, z_d]^T$ be the position vectors of the spacecraft and the disturbing body, as shown in Figure 1. Then, the disturbing function D is written as

$$D = \mu_d \left(\frac{1}{\Delta} - \frac{x x_d + y y_d + z z_d}{r_d^3} \right) \tag{4}$$

where μ_d is the gravitational constant of the disturbing body; $r_d = \|\boldsymbol{r}_d\|$ denotes the distance of the disturbing body from the central body; and Δ is the distance between the spacecraft and the disturbing body, written as

$$\Delta^2 = (x - x_d)^2 + (y - y_d)^2 + (z - z_d)^2 \tag{5}$$

The differentiation of the disturbing function D is given as [15]

$$\begin{cases} \dfrac{\partial D}{\partial x} = -\mu_d \left(\dfrac{x - x_d}{\Delta^3} + \dfrac{x_d}{r_d^3} \right) \\ \dfrac{\partial D}{\partial y} = -\mu_d \left(\dfrac{y - y_d}{\Delta^3} + \dfrac{y_d}{r_d^3} \right) \\ \dfrac{\partial D}{\partial z} = -\mu_d \left(\dfrac{z - z_d}{\Delta^3} + \dfrac{z_d}{r_d^3} \right) \end{cases} \tag{6}$$

Assume that the radial, circumferential and normal direction cosines of the spacecraft are represented by (l_1, m_1, n_1), (l_2, m_2, n_2) and (l_3, m_3, n_3), given by

$$\begin{cases} l_1 = \cos\Omega \cos u - \sin\Omega \sin u \cos i \\ m_1 = \sin\Omega \cos u + \cos\Omega \sin u \cos i \\ n_1 = \sin u \sin i \end{cases} \tag{7}$$

$$\begin{cases} l_2 = -\cos\Omega \sin u - \sin\Omega \cos u \cos i \\ m_2 = -\sin\Omega \sin u + \cos\Omega \cos u \cos i \\ n_2 = \cos u \sin i \end{cases} \tag{8}$$

$$\begin{cases} l_3 = \sin\Omega \sin i \\ m_3 = -\cos\Omega \sin i \\ n_3 = \cos i \end{cases} \tag{9}$$

Thus, we have $x = rl_1$, $y = rm_1$, $z = rn_1$. Note that Eqs. (7)-(9) are the components of rotational matrices. In the same way, the position vector of the disturbing body is written as

$$\begin{cases} x_d = r_d \left(\cos\Omega_d \cos u_d - \sin\Omega_d \sin u_d \cos i_d\right) \\ y_d = r_d \left(\sin\Omega_d \cos u_d + \cos\Omega_d \sin u_d \cos i_d\right) \\ z_d = r_d \sin u_d \sin i_d \end{cases} \tag{10}$$

Assume that ϕ denotes the planet displacement angle between the spacecraft and the distributing body measured from the central body, as shown in Figure 1. Let $u_d = \omega_d + \Omega_d$; then, Eq. (5) can be rewritten as

$$\Delta^2 = r^2 + r_d^2 - 2rr_d \cos\phi \tag{11}$$

where $\cos\phi = A\cos u + B\sin u$. For a leading orbit, $\phi < 0$, and for a trailing orbit, $\phi > 0$. Using the small inclination assumption, A and B can be approximated as

$$\begin{aligned} A &= \cos u_d \cos\left(\Omega - \Omega_d\right) + \sin u_d \cos i_d \sin\left(\Omega - \Omega_d\right) \\ &\approx \cos\left(\Omega - \Omega_d - u_d\right) \end{aligned} \tag{12}$$

$$\begin{aligned} B = &\cos i \left[-\sin\left(\Omega - \Omega_d\right)\cos u_d + \cos i_d \sin u_d \cos\left(\Omega - \Omega_d\right)\right] \\ &+ \sin i \sin u_d \sin i_d \\ &\approx -\sin\left(\Omega - \Omega_d - u_d\right) \end{aligned} \tag{13}$$

Note that in Eq. (13)), the term $\sin i \sin u_d \sin i_d$ is ignored as $|\cos i| \gg |\sin i|$ under the assumption of $i \approx 0$. For a spacecraft on a PDO, the radial distance of the disturbing body can be approximated by that of the spacecraft. Then, Eq. (11) can be further simplified as

$$\Delta^2 = 2r^2(1 - \cos\phi) \tag{14}$$

Substituting Eq. (14) into Eq. (6) yields

$$\begin{cases} \dfrac{\partial D}{\partial x} = -\dfrac{\mu_d}{r^3}\left[krl_1 + (1-k)r_d l_d\right] = -\dfrac{\mu_d}{r^2}\left[kl_1 + (1-k)l_d\right] \\ \dfrac{\partial D}{\partial y} = -\dfrac{\mu_d}{r^3}\left[krm_1 + (1-k)r_d m_d\right] = -\dfrac{\mu_d}{r^2}\left[km_1 + (1-k)m_d\right] \\ \dfrac{\partial D}{\partial z} = -\dfrac{\mu_d}{r^3}\left[krn_1 + (1-k)r_d n_d\right] = -\dfrac{\mu_d}{r^2}\left[kn_1 + (1-k)n_d\right] \end{cases} \tag{15}$$

where k is defined as

$$k = \frac{1}{(2 - 2\cos\phi)^{3/2}} \tag{16}$$

The components of the perturbation acceleration R, S and W can be represented in terms of the disturbing function D by

$$\begin{cases} R = l_1 \dfrac{\partial D}{\partial x} + m_1 \dfrac{\partial D}{\partial y} + n_1 \dfrac{\partial D}{\partial z} \\ S = l_2 \dfrac{\partial D}{\partial x} + m_2 \dfrac{\partial D}{\partial y} + n_2 \dfrac{\partial D}{\partial z} \\ W = l_3 \dfrac{\partial D}{\partial x} + m_3 \dfrac{\partial D}{\partial y} + n_3 \dfrac{\partial D}{\partial z} \end{cases} \tag{17}$$

Combine Eq. (15) with Eq. (17) and use equations $l_1^2 + m_1^2 + n_1^2 = 1$ and $l_1 l_d + m_1 m_d + n_1 n_d = \cos\phi$. Then the radial component R can be simplified as

$$R \approx -\frac{\mu_d}{r^2}\left[k + (1-k)\cos\phi\right] \tag{18}$$

The circumferential component S is then given as

$$S = -\frac{\mu_d}{r^2}\left[k\left(l_1 l_2 + m_1 m_2 + n_1 n_2\right) + (1-k)\left(l_d l_2 + m_d m_2 + m_d m_2\right)\right] \tag{19}$$

Using Eqs. (7) and (10) results in $l_1 l_2 + m_1 m_2 + n_1 n_2 = 0$ and

$$\begin{aligned} l_d l_2 + m_d m_2 + m_d m_2 &= -A\sin u + B\cos u \\ &\approx \cos\left(\frac{\pi}{2} - \phi\right) = \sin\phi \end{aligned} \tag{20}$$

Substituting Eq. (20) into Eq. (19), we have

$$S \approx -\frac{\mu_d}{r^2}(1-k)\sin\phi \tag{21}$$

The normal component W is given by

$$W = -\frac{\mu_d}{r^2}\left[k\left(l_1 l_3 + m_1 m_3 + n_1 n_3\right) + (1-k)\left(l_d l_3 + m_d m_3 + n_d n_3\right)\right] \tag{22}$$

It is found that $l_1 l_3 + m_1 m_3 + n_1 n_3 = 0$ and

$$\begin{aligned} l_d l_3 + m_d m_3 + n_d n_3 &= \sin i\left[\cos u_d \sin\left(\Omega - \Omega_d\right) - \cos i_d \sin u_d \cos\left(\Omega - \Omega_d\right)\right] \\ &\quad + \cos i \sin i_d \sin u_d \\ &\approx \sin i \sin\left(\Omega - \Omega_d - u_d\right) \end{aligned} \tag{23}$$

Then, Eq. (22) can be rewritten as

$$W \approx -\frac{\mu_d}{r^2}(1-k)\sin i \sin\left(\Omega - \Omega_d - u_d\right) \tag{24}$$

Note that although we assume that $i \approx 0$, the $\sin i$ term is still reserved in Eq. (24) for two main reasons. The first is that there doesn't exist a variable that is much larger than $\sin i$ in Eq. (24) (as discussed in section 2 and a different case that ignores the term of $\sin i$ can be found from Eq. (13)). Second, the normal component of the disturbing acceleration is crucial to the changes in i, Ω, and ω (as shown in Eq. (3)): preserving the term of $\sin i$ can improve accuracy in predicting these three elements.

A summary of the above analysis is then given as

$$\begin{cases} R \approx -\dfrac{\mu_d}{r^2}\left[k + (1-k)\cos\phi\right] \\ S \approx -\dfrac{\mu_d}{r^2}(1-k)\sin\phi \\ W \approx -\dfrac{\mu_d}{r^2}(1-k)\sin i \sin\left(\Omega - \Omega_d - u_d\right) \end{cases} \tag{25}$$

Equation (25) is the proposed third-body perturbation model for PDOs. Directly solving the ODEs in Eqs. (3) and (25) is impossible as they are highly nonlinear, and the variables are coupled with each other. In the next section, to resolve the difficulty, a two steps process is proposed to obtain the analytical propagation of PDOs.

4. Analytical Solution of the Planet-Displaced Orbit

Directly solving the ODE in Eq. (3) is impossible as the ODE in Eq. (3) is highly nonlinear, and the variables are coupled with each other. In this study, motivated by the Picard iteration method in solving ODEs, the analytical solution of the ODE in Eq. (3) is iteratively derived. In this section, first, the Picard iteration method is briefly reviewed. Then, the two-step process for obtaining the analytical solution is detailed.

4.1. Picard Iteration Method

Recently, the Picard iteration method has been well investigated to address numerical integration for orbital mechanics. The Picard iteration method can obtain a sequence of approximate solutions of the initial value problem (*e.g.*, orbit propagation problem). Bai and Junkins [43], and Feagin and Nacozy [44] investigated fixed time-step methods using Chebyshev polynomials and Picard iteration. Nakhjiri and Villac further proposed a modified Picard integrator by transforming vector fields to polynomial form and successfully applied their method to numerically integrate trajectories and high-order state transition tensors [45]. Read *et al.* employed a modified Chebyshev Picard iteration method to propagate the orbital elements. Woollands and Junkins developed an adaptive self-tuning Picard-Chebyshev numerical integration method for orbit propagation, which was proven to be more efficient than a high-order Runge-Kutta method [46]. More recently, Singh *et al.* investigated the possibility of using a Picard Chebyshev method to generate quasi-frozen orbits around the Moon [47]. These research studies focus on addressing numerical integration problems. This paper derives the analytical solution of the PDOs using the idea of the Picard iteration method, and the Picard iteration method is briefly described as follows.

Consider a general initial value problem governed by the ODE, given as

$$\begin{cases} \dfrac{d\boldsymbol{x}}{dt} = \boldsymbol{f}\left(\boldsymbol{x}, t\right) \\ \boldsymbol{x}\left(t_0\right) = \boldsymbol{x}_0 \end{cases} \tag{26}$$

where $\boldsymbol{f}\left(\boldsymbol{x}, t\right)$ is a continuous function, which satisfies the Lipschitz condition [45]. Using the Picard iteration method [45], the solution $\boldsymbol{x}\left(t\right)$ can be iteratively

obtained as

$$\begin{aligned}
\boldsymbol{p}_0(t) &= \boldsymbol{x}_0 \\
\boldsymbol{p}_1(t) &= \boldsymbol{x}_0 + \int_{t_0}^{t} \boldsymbol{f}\left[\boldsymbol{p}_0(\tau), \tau\right] d\tau \\
\boldsymbol{p}_2(t) &= \boldsymbol{x}_0 + \int_{t_0}^{t} \boldsymbol{f}\left[\boldsymbol{p}_1(\tau), \tau\right] d\tau \\
&\vdots \\
\boldsymbol{p}_m(t) &= \boldsymbol{x}_0 + \int_{t_0}^{t} \boldsymbol{f}\left[\boldsymbol{p}_{m-1}(\tau), \tau\right] d\tau
\end{aligned} \tag{27}$$

where $\boldsymbol{p}_m(t)$ denotes the approximated solution in the m-th iteration. It has been proved that, as the number of the iterations tends to be infinity, the $\boldsymbol{p}_m(t)$ will converge to the true solution $\boldsymbol{x}(t)$ [46]. The Picard iteration method provides an effective way to solve an ODE problem.

In the context of the current investigation, the variables of the ODEs in Eqs. (3) and (25) are five orbit elements (a, e, i, Ω and ω) and the trailing angle ϕ. These six variables change at slow rates. Hence, to obtain the analytical solution, we first integrate the ODEs in Eq. (3) with respect to the true anomaly θ, assuming that the six variables remain constant during the time of integration (*i.e.*, step $\boldsymbol{p}_1(t) = \boldsymbol{x}_0 + \int_{t_0}^{t} \boldsymbol{f}\left[\boldsymbol{p}_0(\tau), \tau\right] d\tau$ in Eq. (27)). Then, re-substitute the solution in the first iteration into the ODEs, and the analytical solution of the second iteration (step) is integrated (*i.e.*, step $\boldsymbol{p}_2(t) = \boldsymbol{x}_0 + \int_{t_0}^{t} \boldsymbol{f}\left[\boldsymbol{p}_1(\tau), \tau\right] d\tau$ in Eq. (27)). Through numerical simulations, it is found that the solution in the second step is accurate enough (see Sec. 5.1). The detailed process and result of the two iterations are respectively given in subsections 4.2 and 4.3.

4.2. Analytical Solution Considering Constant Planet Displacement Angle

4.2.1. Solution of the semi-major axis

The variables n and k are constant if we assume that a, e, i, Ω, ω and ϕ remain constant. Then, using the relation $u \approx u_d$ (obtained from $a \approx a_d$), the

ODE of the semi-major axis a is given as

$$\begin{aligned}\frac{da}{d\theta} &= -\frac{2\mu_d}{n^2a^2\left(1-e^2\right)}\{[k+(1-k)\cos\phi]e\sin\theta+(1+e\cos\theta)(1-k)\sin\phi\}\\ &\approx -\frac{2\mu_d}{n_d^2a_0^2\left(1-e_0^2\right)}\left(1-k_0\right)\sin\phi_0\end{aligned} \tag{28}$$

where

$$k_0 = \frac{1}{\left(2-2\cos\phi_0\right)^{3/2}} \tag{29}$$

Then the solution of the ODE in Eq. (28) is derived as:

$$a_{1\mathrm{s}} = a_0 + k_a\left(\theta-\theta_0\right) \tag{30}$$

where the subscript 1s represents the solution of the first step (*i.e.*, the step under constant assumptions) and

$$k_a = -\frac{2\mu_d}{n_d^2a_0^2\left(1-e_0^2\right)}\left(1-k_0\right)\sin\phi_0 \tag{31}$$

4.2.2. Solution of the eccentricity

Substituting the expressions for radial and circumferential perturbation acceleration components from Eq. (25) into Eq. (3) and using the equation $\cos E = \frac{\cos\theta+e}{1+e\cos\theta}$ leads to

$$\begin{aligned}\frac{de}{d\theta} \approx &-\frac{\mu_d\sqrt{1-e_0^2}}{n_d^2a_0^3}\left[k_0+(1-k_0)\cos\phi_0\right]\sin\theta\\ &-\frac{\mu_d\sqrt{1-e_0^2}}{n_d^2a_0^3}\left(1-k_0\right)\sin\phi_0\left(\cos\theta+\frac{\cos\theta+e_0}{1+e_0\cos\theta}\right)\end{aligned} \tag{32}$$

Integrating Eq. (32) with respect to the independent variable θ over one revolution results in

$$\Delta e = -\frac{\mu_d\sqrt{1-e_0^2}}{n_d^2a_0^3}\left(1-k_0\right)\sin\phi_0\int_0^{2\pi}\frac{\cos\theta+e_0}{1+e_0\cos\theta}d\theta \tag{33}$$

Considering that $e_0 \approx 0$, the term $\frac{1}{1+e_0\cos\theta}$ can be approximated using a Tayler expression as

$$\frac{1}{1+e_0\cos\theta} \approx 1-\cos\theta e_0+\cos^2\theta e_0^2-\cos^3\theta e_0^3+\cos^4\theta e_0^4+\cdots \tag{34}$$

By using the approximation from Eq. (34), the integration in Eq. (33) can be rewritten as

$$\Delta e \approx -\frac{\pi \mu_d \sqrt{1-e_0^2}}{n_d^2 a_0^3} (1-k_0) \sin\phi_0 \left(3e_0 + \frac{3}{4}e_0^3 - \frac{3}{4}e_0^4 + \cdots\right) \tag{35}$$

It can be seen that the change in the eccentricity is very small as e is assumed to be small, and thus the eccentricity can be considered a constant, *i.e.*, $e_{1\mathrm{s}} = e_0$.

4.2.3. Solution of the inclination

By substituting the expressions of the normal acceleration component from Eq. (25) into the derivative of the inclination and using the relation $\theta_d + \omega_d + \Omega_d \approx \theta + \omega + \Omega + \phi$, one obtains

$$\begin{aligned} \frac{di}{d\theta} &\approx -\frac{\mu_d \cos u}{n_d^2 a_0^3 (1 + e_0 \cos\theta)} (1-k_0) \sin i_0 \sin(\Omega_0 - \Omega_d - u_d) \\ &\approx \frac{\mu_d}{n_d^2 a_0^3} (1-k_0) \sin i_0 \cos(\theta + \omega_0) \sin(\theta + \omega_0 + \phi_0) \end{aligned} \tag{36}$$

The solution of the ODE in Eq. (36) is derived as

$$i_{1\mathrm{s}} = \frac{1}{4} k_i^1 \left[2\theta \sin\phi_0 - \cos(2\theta + 2\omega_0 + \phi_0)\right] + \tilde{i}_0 \tag{37}$$

where

$$k_i^1 = \frac{\mu_d \sin i_0 (1-k_0)}{n_d^2 a_0^3} \tag{38}$$

$$\tilde{i}_0 = i_0 - \frac{k_i^1 \left[2\theta_0 \sin\phi_0 - \cos(2\theta_0 + 2\omega_0 + \phi_0)\right]}{4} \tag{39}$$

4.2.4. Solution of the RAAN

Similar to Eq. (36), the derivative of the RAAN with respect to θ is written as

$$\begin{aligned} \frac{d\Omega}{d\theta} &\approx \frac{\mu_d}{n_d^2 a_0^3 (1 + e_0 \cos\theta)} (1-k_0) \sin(\Omega_0 - \Omega_d - u_d) \sin u \\ &\approx \frac{\mu_d}{n_d^2 a_0^3} (1-k_0) \sin(\theta + \omega_0) \sin(\theta + \omega_0 + \phi_0) \end{aligned} \tag{40}$$

and the corresponding solution is obtained as

$$\Omega_{1\mathrm{s}} = \frac{1}{4} k_\Omega^1 \left[2\theta \cos\phi_0 - \sin(2\theta + 2\omega_0 + \phi_0)\right] + \tilde{\Omega}_0 \tag{41}$$

where

$$k_{\Omega}^{1} = \frac{\mu_d}{n_d^2 a_0^3}\left(1 - k_0\right) \tag{42}$$

$$\tilde{\Omega}_0 = \Omega_0 - \frac{1}{4}k_{\Omega}^{1}\left[2\theta\cos\phi_0 - \sin\left(2\theta + 2\omega_0 + \phi_0\right)\right] \tag{43}$$

4.2.5. Solution of the argument of periapsis

Using the expressions for the radial, circumferential, and normal acceleration components from Eq. (25), the ODE of the argument of periapsis in Eq. (3) can be rewritten as

$$\frac{d\omega}{d\theta} \approx k_{\omega}^{1,R}\cos\theta + k_{\omega}^{1,S}\sin\theta + k_{\omega}^{1,W}\sin\left(\omega_0 + \theta + \phi_0\right)\sin\left(\omega_0 + \theta\right) \tag{44}$$

where

$$k_{\omega}^{1,R} = \frac{\mu_d}{n_d^2 a_0^3 e_0}\left[k_0 + \left(1 - k_0\right)\cos\phi_0\right] \tag{45}$$

$$k_{\omega}^{1,S} = -\frac{2\mu_d}{n_d^2 a_0^3 e_0}\left(1 - k_0\right)\sin\phi_0 \tag{46}$$

$$k_{\omega}^{1,T} = -\frac{2\mu_d}{n_d^2 a_0^3 e_0}\left(1 - k_0\right)\sin\phi_0 \tag{47}$$

The analytical solution for the ODE in Eq. (44) is derived as

$$\begin{aligned}\omega_{1\mathrm{s}} = {} & k_{\omega}^{1,R}\sin\theta - k_{\omega}^{1,S}\cos\theta \\ & + \frac{1}{4}k_{\omega}^{1,W}\left[2\theta\cos\left(\phi_0\right) - \sin\left(2\theta + 2\omega_0 + \phi_0\right)\right] + \tilde{\omega}_0\end{aligned} \tag{48}$$

where

$$\begin{aligned}\tilde{\omega}_0 = {} & \omega_0 - k_{\omega}^{1,R}\sin\theta_0 + k_{\omega}^{1,S}\cos\theta_0 \\ & - \frac{1}{4}k_{\omega}^{1,W}\left[2\theta_0\cos\left(\phi_0\right) - \sin\left(2\theta_0 + 2\omega_0 + \phi_0\right)\right]\end{aligned} \tag{49}$$

4.2.6. Solution of the planet displacement angle

Using the near-circular orbit assumption, we have $e \approx 0$, and then the mean angular motion n is approximated as

$$\begin{aligned}n &= \sqrt{\frac{\mu}{a^3}}\frac{\left(1 + e\cos\theta\right)^2}{\left(1 - e^2\right)^{3/2}} \approx \sqrt{\frac{\mu}{a^3}}\left(1 + e\cos\theta\right)^2 \\ &= \sqrt{\frac{\mu}{a^3}}\left(1 + 2e\cos\theta + e^2\cos^2\theta\right) \approx \sqrt{\frac{\mu}{a^3}}\left(1 + 2e\cos\theta\right)\end{aligned} \tag{50}$$

where μ denotes the gravitational constant of the central body.

Then, the ODE of the planet displacement angle ϕ is written as

$$\begin{aligned}\dot{\phi} &= \frac{d\phi}{dt} \approx n_d - n \\ &\approx \frac{\sqrt{\mu}}{a_d^{3/2}}\left(1 + 2e_d\cos\theta_d\right) - \frac{\sqrt{\mu}}{a^{3/2}}(1 + 2e\cos\theta)\end{aligned} \tag{51}$$

Note that $a \approx a_d$, and an approximation is obtained as

$$\frac{\sqrt{\mu}}{a_d^{3/2}} - \frac{\sqrt{\mu}}{a^{3/2}} \approx \frac{3}{2}\frac{\sqrt{\mu}}{a_d^{5/2}}\left(a - a_d\right) \tag{52}$$

Substitution of Eq. (52) into Eq. (51) yields

$$\dot{\phi} \approx \frac{3}{2}\frac{\sqrt{\mu}}{a_d^{5/2}}\left(a - a_d\right) + \frac{\sqrt{\mu}}{a_d^{3/2}}2e_d\cos\theta_d - \frac{\sqrt{\mu}}{a^{3/2}}2e_0\cos\theta \tag{53}$$

Neglecting the influence of the inclination of the spacecraft, the planet displacement angle can be approximated by

$$\phi \approx \theta_d + \omega_d + \Omega_d - \theta - \omega - \Omega \tag{54}$$

Using Eqs. (51) and (54), Eq. (53) can be rewritten as

$$\begin{aligned}\dot{\phi} \approx{}& \frac{3}{2}\frac{\sqrt{\mu}}{a_d^{5/2}}\left(k_a\theta - k_a\theta_0 + a_0 - a_d\right) \\ &+ \frac{\sqrt{\mu}}{a_d^{3/2}}2e_d\cos(\theta + \varphi) - \frac{\sqrt{\mu}}{a_d^{3/2}}2e_0\cos\theta\end{aligned} \tag{55}$$

where

$$\begin{aligned}\varphi &= \omega + \Omega + \phi - \omega_d - \Omega_d \\ &\approx \omega_0 + \Omega_0 + \phi_0 - \omega_d - \Omega_d\end{aligned} \tag{56}$$

Using the relation $n \approx n_d$, the derivative of the planet displacement angle ϕ with respect to the time t is replaced by the derivative with respect to θ as

$$\begin{aligned}\frac{d\phi}{d\theta} = \frac{d\phi}{dt}\frac{dt}{d\theta} \approx{}& \frac{3}{2}\frac{\sqrt{\mu}}{n_d a_d^{5/2}}\left(k_a\theta - k_a\theta_0 + a_0 - a_d\right) \\ &+ \frac{\sqrt{\mu}}{n_d a_d^{3/2}}2e_d\cos(\theta + \varphi) - \frac{\sqrt{\mu}}{n_d a_d^{3/2}}2e_0\cos\theta\end{aligned} \tag{57}$$

The analytical solution of the ODE in Eq. (57) is given as

$$\phi_{1\mathrm{s}} = k_1\theta^2 + k_2\theta + k_3\sin(\theta + \varphi) + k_4\sin\theta + \tilde{\phi}_0 \tag{58}$$

where

$$\tilde{\phi}_0 = \phi_0 - k_1\theta_0^2 - k_2\theta_0 - k_3 \sin(\theta_0 + \varphi) - k_4 \sin\theta_0 \tag{59}$$

$$k_1 = \frac{3\sqrt{\mu}k_a}{4n_d a_d^{5/2}} \tag{60}$$

$$k_2 = \frac{3\sqrt{\mu}\,(a_0 - a_d - k_a\theta_0)}{2n_d a_d^{5/2}} \tag{61}$$

$$k_3 = \frac{2e_d\sqrt{\mu}}{n_d a_d^{3/2}} \tag{62}$$

$$k_4 = -\frac{2e_0\sqrt{\mu}}{n_d a_d^{3/2}} \tag{63}$$

Equations (30), (35), (37), (41), (48) and (58) are the obtained first-step analytical solution for the six considered variables. Based on the results obtained in subsection 4.2, a more accurate analytical solution of the six variables is derived in the next subsection.

4.3. Analytical Solution Considering Changeable Planet Displacement Angle

Using the analysis in subsection 4.2, we have (for the case of ETOs) the following equations:

$$\frac{da}{d\theta} \sim \frac{\mu_d}{n_d^2 a_0^2} \sim 10^2 \text{ (km/rad)} \tag{64}$$

$$\frac{d\phi}{d\theta} \sim \frac{\mu_d\sqrt{\mu}}{n_d^3 a_0^{9/2}}\theta \sim 10^{-4} \text{ (rad/rad)} \tag{65}$$

$$\frac{de}{d\theta} \sim \frac{\mu_d}{n_d^2 a_0^3} \sim 10^{-6} \text{ (1/rad)} \tag{66}$$

$$\frac{di}{d\theta} \sim \frac{\mu_d}{n_d^2 a_0^3} \sim 10^{-6} \text{ (rad/rad)} \tag{67}$$

$$\frac{d\Omega}{d\theta} \sim \frac{\mu_d}{n_d^2 a_0^3} \sim 10^{-6} \text{ (rad/rad)} \tag{68}$$

$$\frac{d\omega}{d\theta} \sim \frac{\mu_d}{n_d^2 a_0^3 e_0} \sim 10^{-4} \text{ (rad/rad)} \tag{69}$$

One can see from Eqs. (64)-(69)) that the changes in the eccentricity, inclination, and RAAN are two orders of magnitude smaller than the changes in the other three variables. Thus, in the second step, we focus on solving the ODEs of the semi-major axis, the planet displacement angle, and the argument of periapsis. The eccentricity, inclination, and RAAN are assumed to remain constant during the analysis.

4.3.1. Solution of the semi-major axis

In the second iteration, the planet displacement angle ϕ, as well as the temporary variable k, are considered changeable variables, which makes the ODE of the semi-major axis difficult to solve. In this study, a polynomial approximation method is used to simplify the derivation process. The term $(1-k)\sin\phi$ is approximated using a third-order polynomial based on the planet displacement angle ϕ as

$$\begin{aligned}(1-k)\sin\phi &= \sin\phi - \frac{\sin\phi}{(2-2\cos\phi)^{3/2}} \\ &\approx \alpha_0 + \alpha_1\phi + \alpha_2\phi^2 + \alpha_3\phi^3\end{aligned} \tag{70}$$

where α_0, α_1, α_2 and α_3 are the coefficients of the polynomial. These coefficients can be obtained using a least square method in a given interval of ϕ or performing a Tayler series expansion in terms of the initial planet displacement angle ϕ_0. We select the cubic polynomial here to approximate the term $(1-k)\sin\phi$ with a trial-and-error procedure. It is adequate for the problem resolved in this paper. A higher-order approximation will complicate the solution while not offering obvious improvement. The readers can employ a lower or higher approximation for other specific scenarios, and the derivation process is similar to that in this paper. By substituting Eqs. (58) and (70) into the ODE of the semi-major axis from Eq. (28), and comprising only secular terms, the

analytical solution of the semi-major axis can be obtained as

$$a_{2\mathrm{s}} = a_0 + \kappa_a \sum_{l=1}^{7} P_l \Delta\theta^l \tag{71}$$

where the subscript 2s represents the solution of the second step, $\Delta\theta = \theta - \theta_0$, $\kappa_a = -\frac{2\mu_d}{n_0^2 a_0^2\left(1-e_0^2\right)}$ and

$$\begin{cases} P_1 = \alpha_0 + \tilde{\phi}_0\left(\alpha_1 + \alpha_2\tilde{\phi}_0 + \alpha_3\tilde{\phi}_0^2\right) \\ P_2 = \dfrac{1}{2}k_2\left(\alpha_1 + 2\alpha_2\tilde{\phi}_0 + 3\alpha_3\tilde{\phi}_0^2\right) \\ P_3 = \dfrac{1}{3}\left(\alpha_1 k_1 + 2\alpha_2 k_1\tilde{\phi}_0 + \alpha_2 k_2^2 + 3\alpha_3 k_1\tilde{\phi}_0^2 + 3\alpha_3 k_2^2\tilde{\phi}_0\right) \\ P_4 = \dfrac{1}{4}k_2\left(2\alpha_2 k_1 + 6\alpha_3 k_1\tilde{\phi}_0 + \alpha_3 k_2^2\right) \\ P_5 = \dfrac{1}{5}k_1\left(\alpha_2 k_1 + 3\alpha_3 k_1\tilde{\phi}_0 + 3\alpha_3 k_2^2\right) \\ P_6 = \dfrac{1}{2}\alpha_3 k_1^2 k_2 \\ P_7 = \dfrac{1}{7}\alpha_3 k_1^3 \end{cases} \tag{72}$$

Equation (71) is the obtained analytical solution for the semi-major axis in the second step.

4.3.2. Solution of the argument of periapsis

For the sake of simplicity, let

$$\mathcal{H} = k_\omega^{1,R}\cos\theta + k_\omega^{1,S}\sin\theta + k_\omega^{1,W}\sin\left(\omega_0 + \theta + \phi_0\right)\sin\left(\omega_0 + \theta\right) \tag{73}$$

which is the expression on the right side of Eq. (44). Note that in Eqs. (2)-(3), the high-order term of $\frac{d\omega}{d\theta}$ is neglected. In the second step, the high-order term is reconsidered to improve accuracy. In this case, we have

$$\frac{d\omega}{d\theta} = \mathcal{H} + \mathcal{H}\frac{d\omega}{d\theta} \tag{74}$$

Then, the derivative of ω w.r.t θ can be approximated as

$$\frac{d\omega}{d\theta} = \frac{\mathcal{H}}{1-\mathcal{H}} = \mathcal{H} + \frac{\mathcal{H}^2}{1-\mathcal{H}} \approx \mathcal{H} + \mathcal{H}^2 \tag{75}$$

With the planet displacement angle ϕ considered as a changeable variable, $\mathcal{H}$ can be rewritten as

$$\begin{aligned}\mathcal{H} = &\frac{\mu_d}{n_d^2 a_0^3 e_0} k_\omega^{2,R} \cos\theta - \frac{2\mu_d}{n_d^2 a_0^3 e_0} k_\omega^{2,S} \sin\theta \\ &- \frac{\mu_d \cos i_0}{n_d^2 a_0^3} k_\omega^{2,W} \sin\left(\omega_0 + \theta + \phi_0\right) \sin\left(\omega_0 + \theta\right)\end{aligned} \tag{76}$$

where $k_\omega^{2,R}$, $k_\omega^{2,S}$, and $k_\omega^{2,W}$ are functions of the planet displacement angle ϕ. $k_\omega^{2,R}$, $k_\omega^{2,S}$, and $k_\omega^{2,W}$ can be approximated by performing a Taylor series expansion in terms of ϕ_0 as

$$k_\omega^{2,R}(\phi) = k + (1-k)\cos\phi \approx \beta_{R,0} + \beta_{R,1}\left(\phi - \phi_0\right) \tag{77}$$

$$k_\omega^{2,S}(\phi) = (1-k)\sin\phi \approx \beta_{S,0} + \beta_{S,1}\left(\phi - \phi_0\right) \tag{78}$$

$$k_\omega^{2,W}(\phi) = 1 - k \approx \beta_{W,0} + \beta_{W,1}\left(\phi - \phi_0\right) \tag{79}$$

where $\beta_{X,0} = k_\omega^{2,X}\left(\phi_0\right)$ and $\beta_{X,1} = \left.\frac{dk_\omega^{2,X}(\phi)}{d\phi}\right|_{\phi=\phi_0}$, $X \in \{R, S, W\}$.

The explicit expressions for $\beta_{X,0}$ and $\beta_{X,1}$ can be easily obtained from Eqs. (77)-(79), which are not given in this Note for brevity. Equations (77)-(79) are used to integrate the term $\mathcal{H}$ from Eq. (75). For the term $\mathcal{H}^2$, the constant assumption and averaging technique are used to reduce the difficulty of deriving equations. Substituting Eqs. (58) and (77)-(79) into Eq. (76), the analytical solution of the argument of periapsis is finally derived after much simplification (steps not shown for brevity), expressed as

$$\begin{aligned}\omega_{2\mathrm{s}} = &\frac{\mu_d}{n_d^2 a_0^3 e_0} \mathcal{F}_\omega^1(\theta) - \frac{2\mu_d}{n_d^2 a_0^3 e_0} \mathcal{F}_\omega^2(\theta) \\ &- \frac{\mu_d \cos i_0}{n_d^2 a_0^3} \mathcal{F}_\omega^3(\theta) + \mathcal{F}_\omega^4(\theta) + \omega_0'\end{aligned} \tag{80}$$

where

$$\begin{aligned}\mathcal{F}_\omega^1(\theta) = &\left[\beta_{R,0} + \beta_{R,1}k_1\left(\theta^2 - 2\right) + \beta_{R,1}k_2\theta + \beta_{R,1}\tilde{\phi}_0 - \beta_{R,1}\phi_0\right]\sin\theta \\ &- \frac{1}{4}\beta_{R,1}\left[k_4 + k_4\cos 2\theta + k_3\cos(\varphi + 2\theta) - 2k_3\theta\sin\varphi\right] \\ &+ \beta_{R,1}\left(2k_1\theta + k_2\right)\cos\theta\end{aligned} \tag{81}$$

$$\begin{aligned}\mathcal{F}_{\omega}^{2}(\theta)=&\frac{1}{4}\beta_{S,1}\left[4\sin\theta\left(2k_1\theta+k_2\right)-k_3\sin(\varphi+2\theta)+2k_4\theta-k_4\sin 2\theta\right]\\&-\left[\beta_{S,0}+\beta_{S,1}\left(k_1\theta^2-2k_1+k_2\theta+\tilde{\phi}_0-\phi_0\right)\right]\cos\theta\\&+\frac{1}{2}\beta_{S,1}k_3\theta\cos\varphi\end{aligned}\tag{82}$$

$$\begin{aligned}\mathcal{F}_{\omega}^{3}(\theta)=&-\frac{1}{8}\sin\left(\phi_0+2\theta+2\omega_0\right)\left[2\beta_{W,0}+\beta_{W,1}k_1\left(2\theta^2-1\right)+2\beta_{W,1}\left(k_2\theta+\tilde{\phi}_0-\phi_0\right)\right]\\&+\frac{1}{12}\theta\cos\phi_0\left[6\beta_{W,0}+\beta_{W,1}\left(2k_1\theta^2+3k_2\theta+6\tilde{\phi}_0-6\phi_0\right)\right]-\frac{1}{8}\beta_{W,1}\left(2k_1\theta+k_2\right)\cos\left(\phi_0+2\theta+2\omega_0\right)\\&+\frac{1}{12}\beta_{W,1}k_3\left[-6\cos\left(\varphi-\omega_0\right)\cos\left(\phi_0+\theta+\omega_0\right)+\cos\left(\varphi+\phi_0+3\theta+2\omega_0\right)-3\cos\left(\varphi-\phi_0+\theta\right)\right]\\&+\frac{1}{12}\beta_{W,1}k_4\left[-6\cos\left(\omega_0\right)\cos\left(\phi_0+\theta+\omega_0\right)+\cos\left(\phi_0+3\theta+2\omega_0\right)-3\cos\left(\phi_0-\theta\right)\right]\end{aligned}\tag{83}$$

$$\mathcal{F}_{\omega}^{4}(\theta)=\frac{1}{2}\left(\frac{\mu_d\beta_{R,0}}{n_d^2a_0^3e_0}\right)^2\theta+\frac{1}{2}\left(\frac{2\mu_d\beta_{S,0}}{n_d^2a_0^3e_0}\right)^2\theta+\frac{1}{4}\left(\frac{\mu_d\cos i_0}{n_d^2a_0^3}\right)^2\theta\tag{84}$$

$$\omega_0'=\omega_0-\frac{\mu_d}{n_d^2a_0^3e_0}\mathcal{F}_{\omega}^{1}\left(\theta_0\right)+\frac{2\mu_d}{n_d^2a_0^3e_0}\mathcal{F}_{\omega}^{2}\left(\theta_0\right)+\frac{\mu_d\cos i_0}{n_d^2a_0^3}\mathcal{F}_{\omega}^{3}\left(\theta_0\right)-\mathcal{F}_{\omega}^{4}\left(\theta_0\right)\tag{85}$$

4.3.3. Solution of the planet displacement angle

By replacing $a_{1\mathrm{s}}$ in Eq. (57) with the expression from Eq. (71), the ODE of the planet displacement angle can be rewritten as

$$\begin{aligned}\frac{d\phi}{d\theta}\approx&\frac{3}{2}\frac{\sqrt{\mu}}{n_da_d^{5/2}}\left(\kappa_a\sum_{l=1}^{7}P_l\Delta\theta^l+a_0-a_d\right)\\&+\frac{\sqrt{\mu}}{n_da_d^{3/2}}2e_d\cos(\theta+\varphi)-\frac{\sqrt{\mu}}{n_da_d^{3/2}}2e_0\cos\theta\end{aligned}\tag{86}$$

Then, the solution of the planet displacement angle ϕ can be obtained by directly integrating Eq. (86), given as

$$\begin{aligned}\phi_{2\mathrm{s}}=&\frac{3}{2}\frac{\kappa_a\sqrt{\mu}}{n_da_d^{5/2}}\sum_{l=1}^{7}\frac{P_l}{l+1}\Delta\theta^{l+1}+\frac{3}{2}\frac{\sqrt{\mu}}{n_da_d^{5/2}}\left(a_0-a_d\right)\Delta\theta\\&+\frac{\sqrt{\mu}}{n_da_d^{3/2}}2e_d\sin(\theta+\varphi)-\frac{\sqrt{\mu}}{n_da_d^{3/2}}2e_0\sin\theta+\phi_0'\end{aligned}\tag{87}$$

where

$$\phi_0' = \phi_0 - 2e_d \sin(\theta_0 + \varphi) \frac{\sqrt{\mu}}{n_d a_d^{3/2}} + 2e_0 \sin\theta_0 \frac{\sqrt{\mu}}{n_d a_d^{3/2}} \tag{88}$$

Therefore, according to Eqs. (71), (80) and (87), and using the relation $\theta \approx \theta_0 + n_0 t$ (under the assumptions that $t_0 = 0$ and $e \approx 0$), the analytical solution in the second-step is expressed as

$$\begin{cases} a_{2\mathrm{s}}(t) = a_0 + \kappa_a \sum_{l=1}^{7} P_l (n_0 t)^l \\ e_{1\mathrm{s}}(t) = e_0 \\ i_{1\mathrm{s}}(t) = \frac{1}{4} k_i^1 \left[2(n_0 t + \theta_0)\sin\phi_0 - \cos(2n_0 t + 2\theta_0 + 2\omega_0 + \phi_0)\right] + \tilde{i}_0 \\ \Omega_{1\mathrm{s}}(t) = \frac{1}{4} k_\Omega^1 \left[2(n_0 t + \theta_0)\cos\phi_0 - \sin(2n_0 t + 2\theta_0 + 2\omega_0 + \phi_0)\right] + \tilde{\Omega}_0 \\ \omega_{2\mathrm{s}}(t) = \frac{\mu_d}{n_d^2 a_0^3 e_0} \mathcal{F}_\omega^1 (n_0 t + \theta_0) - \frac{2\mu_d}{n_d^2 a_0^3 e_0} \mathcal{F}_\omega^2 (n_0 t + \theta_0) \\ \qquad - \frac{\mu_d}{n_d^2 a_0^3} \cos i_0 \mathcal{F}_\omega^3 (n_0 t + \theta_0) + \mathcal{F}_\omega^4 (n_0 t + \theta_0) + \omega_0' \\ \phi_{2\mathrm{s}}(t) = \frac{3\kappa_a \sqrt{\mu}}{2 n_d a_d^{5/2}} \sum_{l=1}^{7} \frac{P_l}{l+1} (n_0 t)^{l+1} + \frac{3\sqrt{\mu}}{2 n_d a_d^{5/2}} (a_0 - a_d) n_0 t \\ \qquad + \frac{2e_d \sqrt{\mu}}{n_d a_d^{3/2}} \sin(n_0 t + \theta_0 + \varphi) - \frac{2e_0 \sqrt{\mu}}{n_d a_d^{3/2}} \sin(n_0 t + \theta_0) + \phi_0' \end{cases} \tag{89}$$

In this paper, the analytical solution refers to the solution from Eq. (89) if no special statements are made.

5. Numerical validation

This section provides two numerical simulations, including an accuracy validation in subsection 5.1 and a feasible range analysis in subsection 5.2. In subsection 5.1, a validation against a single case (*i.e.*, a LISA orbit) is performed, whereas the feasible ranges (*i.e.*, the lower and upper bounds) of the eccentricity, inclination, and planet displacement angle, within which the proposed analytical solution are valid, are discussed in subsection 5.2.

5.1. Accuracy Validation on the Example of LISA Spacecraft

In this subsection, the accuracy of the proposed analytical solution (*i.e.*, Eq. (89)) is validated against the orbit of the Laser Interferometer Space Antenna (LISA) mission. The LISA mission architecture baseline relies on a triangular interferometer aimed at detecting low-frequency gravitational waves, with three spacecraft moving on the ETOs [3, 48, 49]. The Sun and the Earth are taken as the central body and the disturbing body, respectively. The coordinate system defined in section 2 is equivalent to the heliocentric ecliptic inertial coordinate system. The initial Keplerian elements of one LISA spacecraft and the Earth are listed in Table 1. Note the significant figures in Table 1 are provided to ensure reproduce of the results in this paper.

Table 1: Nominal orbit elements of the Earth and spacecraft (AU = 149598022.2906 km) [3]

Object	a, AU	e	i, deg	Ω, deg	ω, deg	θ, deg
Earth	1	0.0167	0.0019	174.8370	288.1487	357.0427
Spacecraft	0.99912043	0.0123	1.0140	63.2793	10.9937	3.0618

The simulation is carried out over 10 years starting at UTC 2015.01.01 00:00:0000. The values of the coefficients α_0, α_1, α_2 and α_3 are listed in Table 2. These coefficients are obtained using the least square method in the interval $\phi \in [\pi/12, \pi/6]$, in which the LISA orbits are located [3]. For LISA orbit, the gravitational perturbation of the Earth is two orders of magnitude larger than that of other planets [50]. Therefore, it is sufficient to propagate the LISA orbit considering the influences of the Sun and Earth. A comparison between the analytical and numerical results is then performed in the presence of Earth's third-body perturbations. The numerical result is obtained by directly integrating the ODEs in Eq. (2) using the Runge-Kutta (4,5) ODE solver [51], with a relative tolerance of 10^{-10} and an absolute tolerance of 10^{-10}. Note that the numerical result is equivalent to the numerical solutions of the ERTBP model as the Earth is assumed to orbit around the Sun in an elliptic orbit.

First, the spacecraft orbit is propagated using both the numerical method and the proposed analytical solution. Figure 2 shows the comparisons of our

Table 2: Coefficients of the third-order polynomial

Coefficient	Value
α_0	-73.8814
α_1	392.4998
α_2	-764.305
α_3	521.7283

analytical solutions with numerical results for the semi-major axis, the argument of periapsis and the planet displacement angle. The black, blue, and red curves represent the solutions obtained from the numerical integration, the first step and the second step, respectively. The numerical evolution trends are well followed by the proposed analytical solution. The time histories of the relative errors (RE) are calculated, and the mean relative errors (MRE) are shown in Table 3. In Table 3, the MREs are calculated as follow:

$$\mathrm{MRE}(\chi) = \sum_{p=0}^{N} \frac{|\chi(t_p) - \tilde{\chi}(t_p)|}{|\chi(t_p)|} \times 100\%, \ \chi \in \boldsymbol{K} \tag{90}$$

where t_0 and t_N represent the initial and final epochs, $t_1, \cdots, t_{N-1}$ are time points selected from (t_0, t_N) (with an interval of 43200 s). One can see from Table 3 that the proposed analytical solutions have an MRE of less than 0.22%. Recall that the first-step analytical solutions of e, i and Ω are accurate enough as they change slowly (as discussed in subsection 4.3). The MREs of the first-step analytical solutions of e, i and Ω are at least one order of magnitude less than that of a. The second-step analytical solutions of e, i and Ω are not derived in this paper, and thus, the corresponding MRE results are not shown in Table 3.

In addition, the position and velocity vectors are calculated based on the numerical and analytical solutions. The time history of the REs of the position and velocity vectors are shown in Figure 3. The REs in Figure 3 are defined as

$$\mathrm{RE}(r_p) = \frac{r_p - \tilde{r}_p}{\|r\|} \times 100\% \tag{91}$$

$$\mathrm{RE}(v_p) = \frac{v_p - \tilde{v}_p}{\|r\|} \times 100\% \tag{92}$$

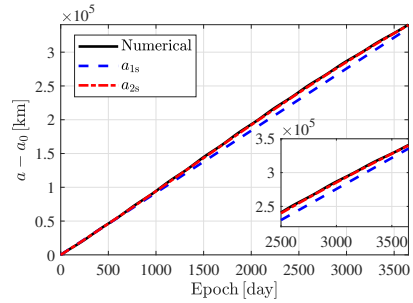

(a) Prediction of the semi-major axis

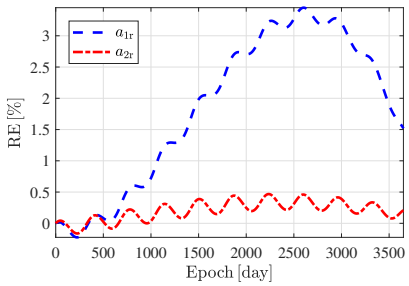

(b) Predicted error of the semi-major axis

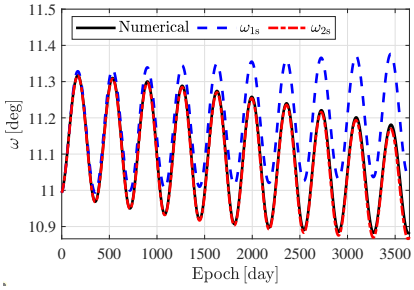

(c) Prediction of the argument of periapsis

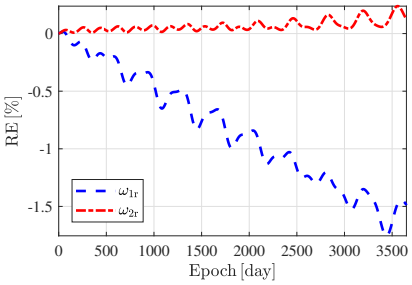

(d) Predicted error of the argument of periapsis

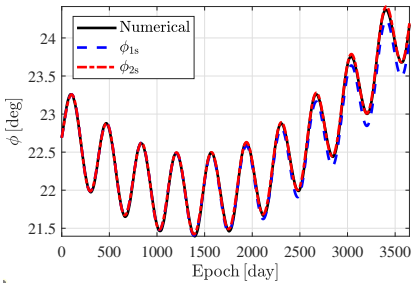

(e) Prediction of the planet displacement angle

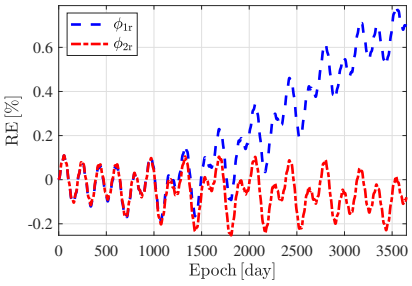

(f) Predicted error of the planet displacement angle

Figure 2: Comparisons between the numerical and analytical solutions.

where the subscript $p \in \{x, y, z\}$, $\boldsymbol{x} = [\boldsymbol{r}; \boldsymbol{v}] = [r_x, r_y, r_z, v_x, v_y, v_z]^T$ and $\tilde{\boldsymbol{x}} = [\tilde{\boldsymbol{r}}; \tilde{\boldsymbol{v}}] = [\tilde{r}_x, \tilde{r}_y, \tilde{r}_z, \tilde{v}_x, \tilde{v}_y, \tilde{v}_z]^T$ denote the Cartesian elements of the numerical and the analytical solutions, respectively. From Figure 3 we can see that the analytical solutions can predict the position and velocity vectors to relative errors of the order of 0.1%.

Note that the intent of this example is to demonstrate the capacity of the

Table 3: Mean relative errors of six variables

Steps	First step	Second step
a	1.8727%	0.2205%
e	0.1970%	-
i	0.0008%	-
Ω	0.0035%	-
ω	0.8389%	0.0667%
ϕ	0.2495%	0.0798%

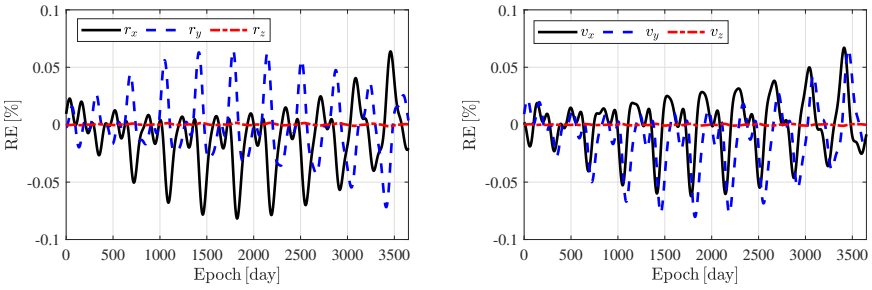

(a) Position (b) Velocity

Figure 3: Relative errors of the analytical solution in predicting Cartesian elements.

proposed analytical solution to accurately propagate the absolute state of PDOs. In practice, for LISA-like space formation, the relative geometry (usually described by the arm length, breathing angle, and relative velocity) of the formation is more critical than the absolute orbits [3, 42, 4]. Additionally, the starting epoch (*i.e.*, 2015) adopted in this example is outdated for the LISA mission, and up-to-date orbital parameters of the LISA mission can be found in [48, 3].

5.2. Feasible Range Analysis

The feasible ranges of the proposed analytical solution are investigated. Note that as the classic orbital elements and Lagrange's planetary equations are employed in this work, the eccentricity cannot be zero. To validate the performance of the proposed analytical solution under small eccentricity, a single example is first presented. When $e_0 = 10^{-8}$ and other orbital elements are fixed as those in Table 1, the results are shown in Figure 4 and Figure 5. It is found that the

ϕ is accurately predicted while the ω is poorly predicted when the eccentricity is very small. This is because in Eq. (80), some components are divided by e_0. However, for the considered ETO with small inclination and eccentricity, its position and velocity are mainly determined by the phase (equivalent to ϕ). The RE of ω is larger than 100% (as seen in Figure 4) while REs of position and velocity are no larger than 0.07% (as seen in Figure 5). Thus, although the argument of periapsis is poorly predicted, its position and velocity elements are still accurately predicted when $e_0 = 10^{-8}$. The singularity related to the classic orbital elements maybe alleviated by considering a different element set (*e.g.*, equinoctial orbit elements), which will be included in our future work.

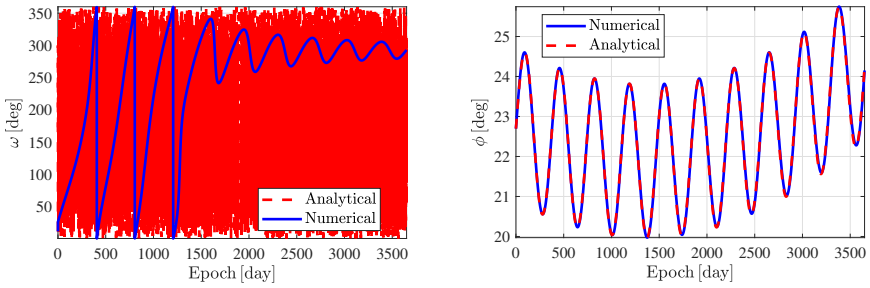

(a) Argument of periapsis (b) Planet displacement angle

Figure 4: Comparisons between the numerical and analytical solutions when $e_0 = 10^{-8}$.

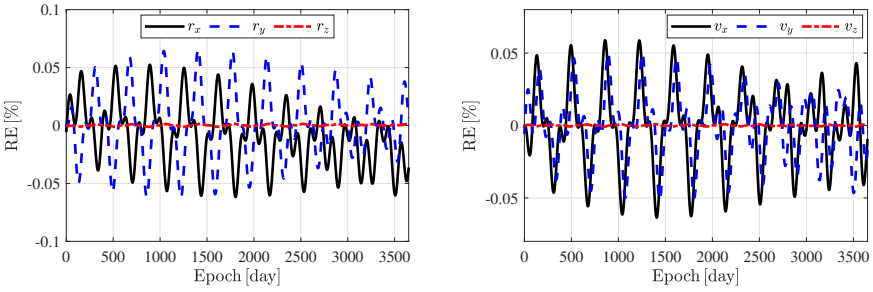

(a) Position (b) Velocity

Figure 5: Relative errors of the analytical solution in predicting Cartesian elements when $e_0 = 10^{-8}$.

Additionally, the MREs of the proposed analytical solution when the initial eccentricity (*i.e.*, e_0) ranges from 10^{-12} to 10^{-4} (the initial values of other five elements are fixed as the corresponding values in Table 1) are presented in Figure 6. Different from Eq. (90), here, the MRE is defined as:

$$\mathrm{MRE} = \frac{1}{6} \sum_{\chi \in \{r_x, r_y, r_z, v_x, v_y, v_z\}} \sum_{p=0}^{N} \frac{|\chi(t_p) - \tilde{\chi}(t_p)|}{|\chi(t_p)|} \times 100\% \tag{93}$$

One can see from Figure 6 that the MRE is approximately 10^{-2} when $e_0 \geq 10^{-10}$. There is a clear turning point at around $e_0 = 10^{-10}$, and the predicted performance seriously degrades when e_0 is smaller than 10^{-10}. For example, when $e_0 = 10^{-12}$, the MRE is 31.15%. Therefore, the lower limit for the eccentricity is set as 10^{-10}.

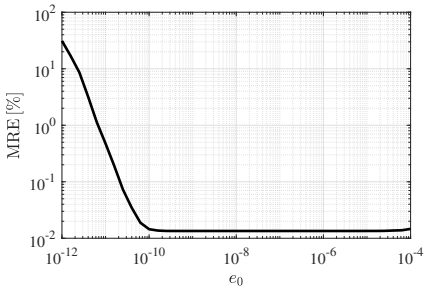

Figure 6: Mean relative errors of the analytical solution in predicting Cartesian elements in the small eccentricity case.

Moreover, recall, in this paper, two major assumptions are made: $e \approx 0$ and $i \approx 0$. In addition, the planet displacement angle ϕ is constrained in the interval $[\pi/12, \pi/6]$, since the coefficients of the polynomial in Eq. (70) are obtained using the samples in $[\pi/12, \pi/6]$. In the following, the influences of these three variables on the accuracy of the analytical solution are analyzed. The spacecraft orbit in Table 1 is taken as a nominal orbit for the analysis. During the analysis, only one parameter (*i.e.*, the eccentricity or inclination or planet displacement angle) is varied at a time, and the other five elements are fixed as the nominal values. The MREs (using Eq. (93)) under different orbital parameters are represented by the black curves in Figure 7.

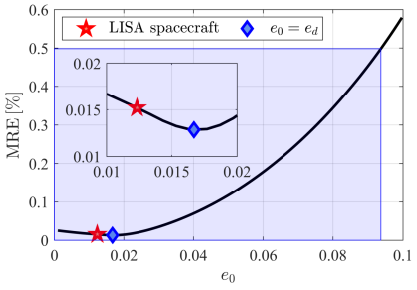

(a) Eccentricity

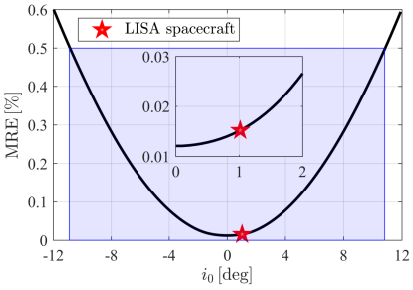

(b) Inclination

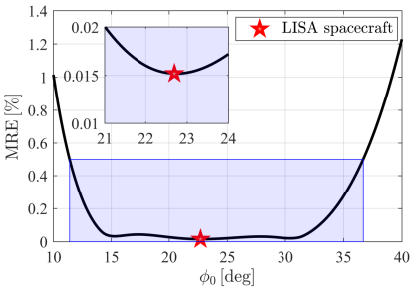

(c) Planet displacement angle

Figure 7: Mean relative errors under different orbital parameters.

Here, an MRE of less than 0.5% is considered as feasible. The feasible ranges for the eccentricity, inclination, and planet displacement angle are shown by the blue rectangles in Figure 7. The detailed bounds of the feasible ranges are listed in Table 4. It should be noted that the feasible range for each individual parameter in Table 4 is only valid when the other five parameters are fixed as nominal values.

Table 4: Feasible ranges of the analytical solution

Variable	Feasible range
Eccentricity	$10^{-10} \leq e_0 \leq 0.094$
Inclination	$-10.9^\circ \leq i_0 \leq 10.8^\circ$
Planet displacement angle	$11.4^\circ \leq \phi_0 \leq 36.7^\circ$

It is also interesting to find that when the eccentricity of the spacecraft is equal to that of the Earth, the analytical solution has the best accuracy. This

is because, in Eqs. (50) and (51) we neglect the quadratic terms $e_d^2 \cos^2 \theta_d$ and $e^2 \cos^2 \theta$, meaning the true anomalies of the Earth and the spacecraft are very close; thus, the two quadratic terms $e_d^2 \cos^2 \theta_d$ and $e^2 \cos^2 \theta$ can offset each other when the eccentricities are equivalent. In this case, the planet displacement angle is approximated with higher precision, and in turn, other variables are better predicted.

6. Application for Planet Displacement Angle-fixed Orbit Design

In this section, the proposed analytical solution is applied to design a planet displacement angle-fixed ETO to show its potential capacity to improve the computational time of orbit design and optimization. The need to design such an orbit comes from the trailing distance constraint due to communication requirements [3]. Note that under the time-varying perturbations, the planet displacement angle of an uncontrolled ETO cannot be fixed. In this paper, *fixed planet displacement angle* means that the changes in the planet displacement angle are as small as possible (*i.e.*, minimize $|\phi_{\max} - \phi_{\min}|$). In addition, the initial planet displacement angle of the designed ETO is fixed as that of the LISA spacecraft in Table 1. According to Eq. (87), the planet displacement angle-fixed ETO should satisfy $e_0 = e_d$, $\theta_0 = \theta_d$, $\omega_0 + \Omega_0 = \omega_d + \Omega_d$ and

$$a_d - a_0 = \kappa_a \sum_{l=1}^{7} \frac{P_l}{l+1} \Delta\theta_f^l \tag{94}$$

In Eq. (94), θ_f denotes the true anomaly. Note that both sides of Eq. (94) contain the variable a_0. In this study, Eq. (94) is solved using the interior trust region approach [52], and we have $a_0 = 149407905.5083$ km. For convenience, let $\omega_0 = 0$ and then we have $\Omega_0 = \omega_d + \Omega_d$. In addition, to neglect the influences of the normal component of the perturbations, the inclination of the planet displacement angle-fixed ETO is set to be 0. The time history of the planet displacement angle of the designed orbit is depicted in Figure 8.

In addition, the Genetic algorithm (GA) [53] is employed to optimize the planet displacement angle-fixed ETO, with the result shown by the red dashed

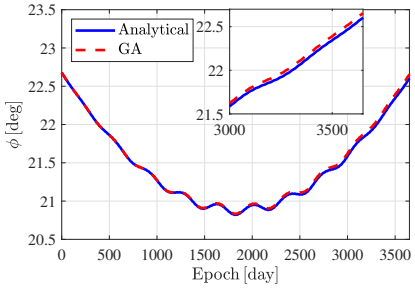

Figure 8: Time histories of the planet displacement angle.

curve as a comparison. During the GA optimization process, the variables being optimized are six orbital elements in Eq. (1), and the objective function is the maximal change in planet displacement angle. The population and the number of generations are set as 100 and 50, respectively. In addition, the Runge-Kutta (4,5) ODE solver is employed for orbit propagation (using the dynamics in Eq. (2)) in the GA optimization process. The results from the proposed analytical solution and GA are listed in Table 5. Compared with GA, the change in the planet displacement angle of the proposed analytical solution increases by approximately 0.68%. However, the time consumption using the analytical solution is less than 0.01% of that of the GA method.

Table 5: Comparisons between the planet displacement angle-fixed orbits obtained by different methods

Method	Analytical solution	GA
Changes in planet displacement angle	1.8590 deg	1.8463 deg
Computational time	0.2321 s	About 45 min

7. Conclusion

The planet displacement angle is the most relevant parameter driving the evolution of planet-displaced orbits (PDOs) under the influence of the leading (or trailing) planet's gravitational field. It can be used to model the third-body perturbation accurately. A two-step process can be used to obtain an analytical

propagation solution by approximating the planet displacement angle. The analytical propagation solution is obtained under the assumption that the PDO has small eccentricity and inclination and has a semi-major axis close to that of the disturbing body. Such an approach, when used to propagate the state of a Laser Interferometer Space Antenna (LISA) spacecraft at the Earth-trailing orbit (ETO), is found to accurately follow the numerical results over a 10-year period with a relative error in predicting the position and velocity vectors no larger than 0.1%. Such an analytical solution is feasible for PDOs whose eccentricity and inclination are smaller than 0.09 and 11 deg, respectively. In addition, the PDO's initial eccentricity should not be smaller than 10^{-10}. The analytical solution can be potentially used to improve the computational time in designing trajectories that requiring a computationally expensive optimization method. In the future, different orbital elements can be considered to alleviate the singularity related to the eccentricity. Moreover, as the accuracy of the proposed propagation solution is demonstrated numerically in this work, some analytical ways should be further developed to evaluate its errors.

Acknowledgments

This work was sponsored by the National Key R&D Program of China (No. 2020YFC2201200).

References

[1] J. B. Pezent, R. Sood, A. Heaton, Configuration space and stability analysis of solar sail near-vertical earth-trailing orbits, Advances in Space Research 67 (9) (2021) 2981–2994. doi:10.1016/j.asr.2020.10.011.

[2] W. Martens, E. Joffre, R. Florian, M. Valerio, Astrodynamics techniques for missions towards Earth-Trailing or Earth-Leading Heliocentric Orbits, in: 7th International Conference on Astrodynamics Tools and Techniques, Oberpfaffenhofen, Germany, 2018.

[3] X. Xie, F. Jiang, J. Li, Design and optimization of stable initial heliocentric formation on the example of LISA, Advances in Space Research 71 (1) (2023) 420–438. doi:10.1016/j.asr.2022.08.084.

[4] D. Qiao, X. Zhou, X. Li, Feasible domain analysis of heliocentric gravitational-wave detection configuration using semi-analytical uncertainty propagation, Advances in Space Research 72 (2023) 4115–4131. doi:10.1016/j.asr.2023.08.011.

[5] D. Qiao, X. Zhou, X. Li, Configuration uncertainty propagation of gravitational-wave observatory using a directional state transition tensor, Chinese Journal of Aeronautics 1 (2024) 1–20. doi:10.1016/j.cja.2024.06.015.

[6] X. Zhou, X. Li, Z. Huo, L. Meng, J. Huang, Near-Earth Asteroid Surveillance Constellation in the Sun-Venus Three-Body System, Space: Science & Technology 2022 (2022) 9864937. doi:10.34133/2022/9864937.

[7] J. B. Pezent, R. Sood, A. Heaton, Innovative Solar Sail Earth-Trailing Trajectories Enabling Sustainable Heliophysics Missions, The Journal of the Astronautical Sciences 67 (4) (2020) 1249–1270. doi:10.1007/s40295-020-00214-3.

[8] B. G. Marchand, K. C. Howell, R. S. Wilson, Improved corrections process for constrained trajectory design in the n-body problem, Journal of Spacecraft and Rockets 44 (4) (2007) 884–897. doi:10.2514/1.27205.

[9] S. Carletta, M. Pontani, P. Teofilatto, Long-term capture orbits for low-energy space missions, Celestial Mechanics and Dynamical Astronomy 130 (7) (2018) 46. doi:10.1007/s10569-018-9843-7.

[10] L. De Leo, M. Pontani, Low-Thrust Orbit Dynamics and Periodic Trajectories in the Earth–Moon System, Aerotecnica Missili & Spazio 101 (2) (2022) 171–183. doi:10.1007/s42496-022-00122-9.

[11] R. J. McKay, M. Macdonald, J. Biggs, C. McInnes, Survey of Highly Non-Keplerian Orbits with Low-Thrust Propulsion, Journal of Guidance, Control, and Dynamics 34 (3) (2011) 645–666. doi:10.2514/1.52133.

[12] A. K. de Almeida Junior, A. F. B. de Almeida Prado, Comparisons between the circular restricted three-body and bi-circular four body problems for transfers between the two smaller primaries, Scientific Reports 12 (1) (2022) 4148. doi:10.1038/s41598-022-08046-x.

[13] S. K. Singh, J. L. Junkins, M. Majji, E. Taheri, Rapid accessibility evaluation for ballistic lunar capture via manifolds: A Gaussian process regression application, Astrodynamics 6 (4) (2022) 375–397. doi:10.1007/s42064-021-0130-0.

[14] K. I. Alvarado, S. K. Singh, Exploration and Maintenance of Homeomorphic Orbit Revs in the Elliptic Restricted Three-Body Problem 11 (5) (2024) 407. doi:10.3390/aerospace11050407.

[15] C. D. Murray, Dynamical Effects of Drag in the Circular Restricted Three-Body Problem: I. Location and Stability of the Lagrangian Equilibrium Points, Icarus 112 (2) (1994) 465–484. doi:/10.1006/icar.1994.1198.

[16] K. C. Howell, D. B. Spencer, Periodic orbits in the restricted four-body problem, Acta Astronautica 13 (8) (1986) 473–479. doi:/10.1016/0094-5765(86)90026-3.

[17] A. Farrés, À. Jorba, Periodic and quasi-periodic motions of a solar sail close to SL1 in the Earth–Sun system, Celestial Mechanics and Dynamical Astronomy 107 (1) (2010) 233–253. doi:10.1007/s10569-010-9268-4.

[18] X. Lin, G. Zhang, Analytical State Propagation for Continuous-Thrust Linear Relative Motion, Journal of Guidance, Control, and Dynamics 45 (10) (2022) 1946–1957. doi:10.2514/1.G006644.

[19] G. Xu, X. Tianhe, W. Chen, T.-K. Yeh, Analytical solution of a satellite orbit disturbed by atmospheric drag, Monthly Notices of the Royal As-

tronomical Society 410 (1) (2011) 654–662. doi:10.1111/j.1365-2966.2010.17471.x.

[20] D. J. Jezewski, An analytic solution for the J2 perturbed equatorial orbit, Celestial mechanics 30 (4) (1983) 363–371. doi:10.1007/BF01375506.

[21] Z. Yang, Y. Luo, V. Lappas, A. Tsourdos, Nonlinear Analytical Uncertainty Propagation for Relative Motion near J2-Perturbed Elliptic Orbits, Journal of Guidance, Control, and Dynamics 41 (4) (2017) 888–903. doi:10.2514/1.G003071.

[22] H. Peng, X. Bai, Gaussian Processes for improving orbit prediction accuracy, Acta Astronautica 161 (2019) 44–56. doi:10.1016/j.actaastro.2019.05.014.

[23] J. Feng, R. Armellin, X. Hou, Orbit propagation in irregular and uncertain gravity field using differential algebra, Acta Astronautica 161 (2019) 338–347. doi:/10.1016/j.actaastro.2019.05.045.

[24] E. L. Jenson, D. J. Scheeres, Bounding nonlinear stretching about spacecraft trajectories using tensor eigenpairs, Acta Astronautica 214 (2024) 159–166. doi:/10.1016/j.actaastro.2023.10.013.

[25] G. E. Cook, Luni-Solar Perturbations of the Orbit of an Earth Satellite, Geophysical Journal of the Royal Astronomical Society 6 (3) (1962) 271–291. doi:10.1111/j.1365-246X.1962.tb00351.x.

[26] S. N. Paul, B. D. Little, C. Frueh, Detection of Unknown Space Objects Based on Optimal Sensor Tasking and Hypothesis Surfaces Using Variational Equations, The Journal of the Astronautical Sciences 69 (4) (2022) 1179–1215. doi:10.1007/s40295-022-00333-z.

[27] G. Zhang, D. Zhou, X. Bai, Tangent orbital rendezvous with the same direction of terminal velocities, Journal of Guidance, Control, and Dynamics 35 (1) (2012) 335–340. doi:10.2514/1.54586.

[28] D. Zhou, G. Zhang, A solution to two-point boundary value problem for power-limited rendezvous with constant thrust, Acta Astronautica 69 (3-4) (2011) 150–157. doi:10.1016/j.actaastro.2011.03.013.

[29] S. Hernandez, M. R. Akella, Energy-conserving planar spacecraft motion with constant-thrust acceleration, Journal of Guidance, Control, and Dynamics 38 (12) (2015) 2309–2323. doi:10.2514/1.G000972.

[30] H. S. Tsien, Take-Off from Satellite Orbit, Journal of the American Rocket Society 23 (4) (1953) 233–236. doi:10.2514/8.4599.

[31] D. Izzo, F. Biscani, Explicit Solution to the Constant Radial Acceleration Problem, Journal of Guidance, Control, and Dynamics 38 (4) (2014) 733–739. doi:10.2514/1.G000116.

[32] J. L. Gonzalo, C. Bombardelli, Multiple scales asymptotic solution for the constant radial thrust problem, Celestial Mechanics and Dynamical Astronomy 131 (8) (2019) 37. doi:10.1007/s10569-019-9915-3.

[33] D. J. Benney, Escape From a Circular Orbit Using Tangential Thrust, Journal of Jet Propulsion 28 (3) (1958) 167–169. doi:10.2514/8.7261.

[34] F. M. Perkins, Flight Mechanics of Low-Thrust Spacecraft, Journal of the Aerospace Sciences 26 (5) (1959) 291–297. doi:10.2514/8.8048.

[35] P. Gurfil, Spacecraft Rendezvous Using Constant-Magnitude Low Thrust, Journal of Guidance, Control, and Dynamics 46 (11) (2023) 2183–2191. doi:10.2514/1.G007472.

[36] T. S. No, O. C. Jung, Analytical solution to perturbed geosynchronous orbit, Acta Astronautica 56 (7) (2005) 641–651. doi:/10.1016/j.actaastro.2004.11.008.

[37] X. Hou, X. Xin, A Note on the Spin–Orbit, Spin–Spin, and Spin–Orbit–Spin Resonances in the Binary Minor Planet System, The Astronomical Journal 154 (6) (2017) 257. doi:10.3847/1538-3881/aa96ab.

[38] S. Zhao, H. Lei, Lie-series transformations and applications to construction of analytical solutions (2023). doi:10.21203/rs.3.rs-2523599/v1.

[39] H. C. Ko, D. J. Scheeres, Essential Thrust-Fourier-Coefficient Set of Averaged Gauss Equations for Orbital Mechanics, Journal of Guidance, Control, and Dynamics 37 (4) (2014) 1236–1249. doi:10.2514/1.62407.

[40] G. Xu, T. Xu, T.-K. Yeh, W. Chen, Analytical solution of a satellite orbit disturbed by lunar and solar gravitation, Monthly Notices of the Royal Astronomical Society 410 (1) (2011) 645–653. doi:10.1111/j.1365-2966.2010.17470.x.

[41] T. Nie, P. Gurfil, Resonant Control of Satellite Orbits, Journal of Guidance, Control, and Dynamics 44 (12) (2021) 2126–2142. doi:10.2514/1.G006040.

[42] F. Jia, X. Li, D. Qiao, X. Zhou, Semi-analytical configuration optimization of geocentric gravitational wave observatory, Acta Astronautica 202 (2023) 522–534. doi:/10.1016/j.actaastro.2022.10.048.

[43] X. Bai, J. L. Junkins, Modified Chebyshev-Picard Iteration Methods for Orbit Propagation, The Journal of the Astronautical Sciences 58 (4) (2011) 583–613. doi:10.1007/BF03321533.

[44] T. Feagin, P. Nacozy, Matrix formulation of the Picard method for parallel computation, Celestial mechanics 29 (2) (1983) 107–115. doi:10.1007/BF01232802.

[45] N. Nakhjiri, B. Villac, Modified Picard Integrator for Spaceflight Mechanics, Journal of Guidance, Control, and Dynamics 37 (5) (2014) 1625–1637. doi:10.2514/1.G000303.

[46] R. Woollands, J. L. Junkins, Nonlinear Differential Equation Solvers via Adaptive Picard–Chebyshev Iteration: Applications in Astrodynamics, Journal of Guidance, Control, and Dynamics 42 (5) (2019) 1007–1022. doi:10.2514/1.G003318.

[47] S. K. Singh, R. Woollands, E. Taheri, J. Junkins, Feasibility of quasi-frozen, near-polar and extremely low-altitude lunar orbits, Acta Astronautica 166 (2020) 450–468. doi:10.1016/j.actaastro.2019.10.037.

[48] E. Joffre, D. Wealthy, I. Fernandez, C. Trenkel, P. Voigt, T. Ziegler, W. Martens, LISA: Heliocentric formation design for the laser interferometer space antenna mission, Advances in Space Research 67 (11) (2021) 3868–3879. doi:10.1016/j.asr.2020.09.034.

[49] W. Martens, E. Joffre, Trajectory Design for the ESA LISA Mission, The Journal of the Astronautical Sciences 68 (2) (2021) 402–443. doi:10.1007/s40295-021-00263-2.

[50] C. Yang, H. Zhang, Formation flight design for a LISA-like gravitational wave observatory via Cascade optimization, Astrodynamics 3 (2) (2019) 155–171. doi:10.1007/s42064-018-0042-9.

[51] J. R. Dormand, P. J. Prince, A family of embedded Runge-Kutta formulae, Journal of Computational and Applied Mathematics 6 (1) (1980) 19–26. doi:10.1016/0771-050X(80)90013-3.

[52] T. F. Coleman, Y. Li, An Interior Trust Region Approach for Nonlinear Minimization Subject to Bounds, SIAM Journal on Optimization 6 (2) (1996) 418–445. doi:10.1137/0806023.

[53] M. Srinivas, L. M. Patnaik, Genetic algorithms: a survey, Computer 27 (6) (1994) 17–26. doi:10.1109/2.294849.